MOX-Report No. 01/2025

SEIHRDV: a multi-age multi-group epidemiological model and its validation on the COVID-19 epidemics in Italy

Dede', L.; Parolini, N.; Quarteroni, A.; Villani, G.; Ziarelli, G.

MOX, Dipartimento di Matematica
Politecnico di Milano, Via Bonardi 9 - 20133 Milano (Italy)

mox-dmat@polimi.it https://mox.polimi.it

SEIHRDV: a multi-age multi-group epidemiological model and its validation on the COVID-19 epidemics in Italy

Luca Dede'[1,*], Nicola Parolini[1], Alfio Quarteroni[1,2], Giulia Villani[3], and Giovanni Ziarelli[4]

[1]MOX, Department of Mathematics, Politecnico di Milano
[2]Institute of Mathematics, École Polytechnique Fédérale De Lausanne
[3]Department of Mathematics, University of Rome "La Sapienza"
[4]Department of Mathematics, Università degli Studi di Milano
[*]Corresponding author, luca.dede@polimi.it

January 3, 2025

Abstract

We propose a novel epidemiological model, referred to as SEIHRDV, for the numerical simulation of the COVID-19 epidemic, which we validate using data from Italy starting in September 2020. SEIHRDV features the following compartments: Susceptible (S), Exposed (E), Infectious (I), Healing (H), Recovered (R), Deceased (D) and Vaccinated (V). The model is age-stratified, as it considers the population split into 15 age groups. Moreover, it takes into account 7 different contexts of exposition to the infection (family, home, school, work, transport, leisure, other contexts), which impact on the transmission mechanism. Thanks to these features, the model can address the analysis of the epidemics and the efficacy of non-pharmaceutical interventions, as well as possible vaccination strategies and the introduction of the Green Pass, a containment measure introduced in Italy in 2021. By leveraging on the SEIHRDV model, we successfully analyzed epidemic trends during the COVID-19 outbreak from September 2020 to July 2021. The model proved instrumental in conducting comprehensive what-if studies and scenario analyses tailored to Italy and its regions. Furthermore, SEIHRDV facilitated accurate forecasting of the future potential trajectory of the epidemic, providing critical information for informed decision making and public health strategies.

1 Introduction

Coronavirus pandemic was a public health emergency that has affected the whole World since its outbreak in December 2019. Up to December 6, 2023, more than 6.9 million deaths have been registered, and over 770 million cases have been detected according to the World Health Organization. In this context, various mathematical models have been proposed to describe the course of the epidemic and forecast its progression, aiming to assist authorities in selecting optimal control strategies to mitigate the spread of the virus. The primary objective is to prevent the collapse of the healthcare system and ultimately enhance the public health response [1].

Most epidemiological models are derived from the compartmental framework originally proposed by Kermack and McKendrick [2], known as the classic SIR model, which partitions the population into susceptible, infected, and recovered individuals; see also [3]. In recent years, numerous compartmental epidemiological models specifically designed to describe the COVID-19 pandemic have been proposed (see, e.g., [4, 5, 6, 7, 8, 9, 10, 11, 12, 13, 14, 15]). Generally, these models divide the population into subsets, referred to as compartments, that represent different stages of disease progression. The associated mathematical formulations are often deterministic systems of Ordinary Differential Equations (ODEs) governing the mobility of

individuals among compartments. In addition, uncertainty in parameters can be incorporated by reformulating the problem as a set of stochastic differential equations [16, 17]. Beyond compartmental models, various data-driven approaches have emerged. These include agent-based models [18, 19, 20] and machine learning algorithms [21, 22, 23, 24, 25, 26], which offer complementary perspectives for studying the dynamics of infectious diseases.

Building on the foundation of compartmental epidemiological models, the standard SIR model can be generalized to incorporate specific features of the disease under investigation, such as its virological and medical characteristics. Most of these models operate under the assumption of a homogeneous epidemic, disregarding distinctions in factors such as age groups, exposure contexts, and geographical variations that can influence transmission dynamics [27]. While this simplification may reduce the accuracy of forecasts, homogeneous models are computationally efficient, straightforward to calibrate, and often yield results that are interpretable and actionable for policy-making. Since the beginning of the pandemic, we have observed that the impact of COVID-19 infection varies with the age of infected individuals, with clear evidence showing that older people experience more severe outcomes than younger individuals. Additionally, the risk of infection varies depending on the context in which susceptible individuals come into contact with infected persons. Vaccinations, which were widely administered starting in 2021, have significantly impacted the transmission mechanisms of the virus and reduced the severity of symptoms, thereby mitigating the effects of COVID-19 [28].

In this work, we introduce a novel age-stratified ODE-based compartmental model, named SEIHRDV, specifically designed to describe the spread of the Coronavirus epidemic in Italy. This model was applied to analyze the period from September 2020 to July 2021, accounting for varying exposure contexts where infection occurred with differing probabilities, as well as the effects of the vaccination campaign (see e.g., [29]). The model leverages on *Tables of Contacts*, also known as Mossong tables [30], which detail the average daily number of contacts between members of different age groups across various exposure contexts. We consider the following contexts: home, school, work, transport, leisure, and others. As a key innovation, we refined the original *home* category in the Mossong tables by distinguishing between intra-household contacts (*family*) and household-visitor contacts (*home*). This distinction is significant for capturing the impact of Non-Pharmaceutical Interventions (NPIs) that imposed specific restrictions on interactions between relatives and friends visiting different households, as was the case in Italy during certain periods of the first year of the pandemic [31, 32]. This enhanced model enables detailed evaluations of the effects of various NPIs with differing levels of restrictions on social behaviors across 15 age groups and 7 exposure contexts, supporting both retrospective analyses and future scenario projections.

In this paper, we retrospectively assess the effectiveness of restrictions associated with the introduction of the Green Pass, an NPI implemented in Italy in 2021 to maximize vaccination coverage, particularly in public exposure contexts. By incorporating the Green Pass into the model, we aim to simulate a realistic scenario, evaluate its efficacy in reducing infection rates across different contexts, and analyze its impact on the health outcomes of vaccinated individuals.

The paper is organized as follows: in Section 2, we describe the multi-age/multi-context structure of the mathematical model, introducing the different parameters and the way we derived the tables of contacts. Then we describe the calibration process, and how we take into account the vaccination campaign and the introduction of Green Pass restrictions. In Section 3, we show an extensive campaign of numerical results, set in Italy and two Italian administrative regions: Lombardy and Lazio. In Section 4, we draw our conclusions and we discuss possible improvements and possible future extensions of the SEIHRDV.

2 Mathematical model

Starting from the standard SEIR model [33], we develop an ODE-based compartmental model tailored to COVID-19. In Section 2.1, we present the homogeneous SEIHRDV model as a foundational framework. In Section 2.2, we extend this model to incorporate multi-age and multi-context dynamics. Section 2.3 details the implementation of these multi-age and multi-context elements. Finally, in Section 2.4, we outline the

calibration procedure, including the integration of vaccination data and considerations related to the Green Pass policy.

2.1 SEIHRDV model

When a *Susceptible* individual (compartment S) is infected but still in the incubation period, transition to the *Exposed* state (compartment E) occurs. After the incubation period, an Exposed individual becomes *Infected* (compartment I) and can transmit the infection. Before recovery, infected individuals enter the *Healing* state (compartment H), during which they remain positive but are no longer infectious. The progression of the disease ultimately results in either full recovery (*Recovered* compartment R) or death (*Dead* compartment D). To account for the vaccination campaign, we introduce a *Vaccinated* compartment (V), which accounts for individuals who have received at least the first dose of the vaccine. In this work, we neglect the effects of second-dose vaccinations, as our analysis conclude in the summer of 2021, whereas widespread second-dose administration in Italy only began in September 2021. A possible extension of the model, incorporating the complete vaccination cycle, could be inspired by [34].

The SEIHRDV model (cf. Figure 1) is designed to describe all the stages an individual may undergo, from being susceptible to entering the healing phase. The corresponding mathematical model is given by:

$$
\begin{aligned}
&\frac{dS}{dt} = -c\,\beta\,\frac{S\,I}{N} - d\,\frac{S}{S+R} + \mu_R\,R + \mu_V\,V,\\
&\frac{dE}{dt} = c\,\beta\frac{(S+\sigma V)\,I}{N} - \alpha E,\\
&\frac{dI}{dt} = \alpha\,E - \gamma\,I,\\
&\frac{dH}{dt} = \gamma\,I - \omega\,H \qquad\qquad t \in (0,T],\\
&\frac{dR}{dt} = (1-f(S,V))\,\omega\,H - \mu_R\,R,\\
&\frac{dD}{dt} = f(S,V)\omega H,\\
&\frac{dV}{dt} = -\sigma\,c\,\beta\,\frac{V\,I}{N} + d\frac{S}{S+R} - \mu_V\,V,\\
&S(0) = S_0, \quad E(0) = E_0, \quad I(0) = I_0, \quad H(0) = H_0,\\
&R(0) = R_0, \quad D(0) = D_0, \quad V(0) = V_0
\end{aligned}
\tag{1}
$$

where N denotes the total number of individuals of the population that is given by the sum of the number of individuals belonging to one of the 7 compartments, namely $N = S+E+I+H+R+D+V$. Albeit each compartment changes in time, we assume that the total number of individuals N in the population remains constant over time.

The SEIHRDV model is characterized by the following parameters:

- the product $(c\,\beta)$ stands as the transmission rate due to contacts between a susceptible individual and an infected individual, where $\beta : (0,T] \to \mathbb{R}$ is a time-dependent function that captures the variation in contacts, which also depends on the implementation of possible NPIs, while $c : (0,T] \to \mathbb{R}$ embodies changes in the transmission rate, which we will extract from data during the calibration process (cf. Section 2.4.1);
- $\alpha > 0$ denotes the rate at which an exposed individual becomes infectious and is defined as the inverse of the average incubation time;
- $\gamma > 0$ denotes the rate at which an infectious individual becomes unable to infect, but still infected. This rate is derived from the average infectious time;

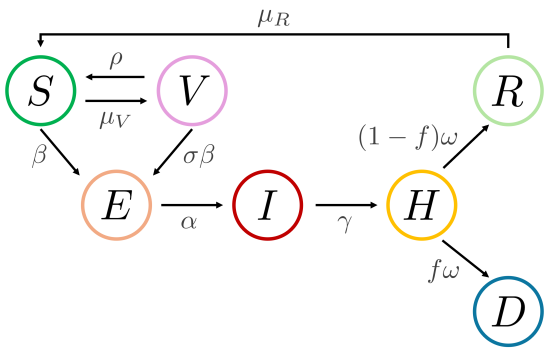

Figure 1: Sketch of SEIHRDV model (S = Susceptible, E = Exposed, I = Infectious, H = Healing, R = Recovered, D = Deceased, V = Vaccinated).

- $\omega > 0$ is a rate derived from the average removal time for deceased, and it is multiplied by f or $1 - f$;
- $\sigma \in [0, 1]$ denotes the inefficacy rate of the vaccine in transmissibility of the disease [35];
- $f : [\tau, T] \to [0, 1]$ is the fatality function, defined as

$$f(t) = f(S(t), V(t); \tau) = \hat{f}\, \frac{S(t-\tau) + \theta\, \sigma\, V(t-\tau)}{S(t-\tau) + \sigma\, V(t-\tau)}, \tag{2}$$

  where $\hat{f}$ is the *infectious fatality rate* ([36]) taken from an Imperial College report of October 2020 [37], and τ is the average elapsing time between the first exposition and death, that we set at 25 days according to clinical studies [38]. We introduce the parameter $\theta \in [0, 1]$ which denotes the rate of inefficacy of the vaccine in the reduction of the severity of the disease. In this way, f is obtained by rescaling the original $\hat{f}$ with the ratio between the sum of individuals susceptible and vaccinated in which the vaccine is not effective either in reducing the transmissibility of the virus or in reducing the severity of the disease, and all the individuals who can potentially contract the virus;

- $d \in \mathbb{N}$ is the number of the average of first doses administered daily, estimated from the data made available from Dipartimento di Protezione Civile Italiana[1];
- $\mu_R > 0$ and $\mu_V > 0$ denote the waning immunity rates for Recovered and Vaccinated individuals respectively, i.e. the rate at which Recovered individuals and Vaccinated individuals, respectively, come back to the susceptible compartment.

In our model, the parameters α, γ, ω, θ, $\hat{f}$, μ_R and μ_V are kept fixed in time, while d, β and σ are instead functions of time. The values of these parameters have been deduced from established studies [28] or directly from available data. Following the methodology in [39], we estimate the initialization of compartments that are not directly accessible from the data provided by the Dipartimento di Protezione Civile Italiana[2], such as the Exposed and Infected individuals. This estimation is obtained thanks to algebraic relationships among measurable quantities, including the CFR (Case Fatality Rate), IFR (Infection Fatality Rate) [37], and the recorded number of deceased individuals. The number of delivered doses d in (1) is rescaled by the factor $\frac{S}{S+R}$ in order to take into account that a portion of doses are administered to both detected and undetected recovered individuals.

[1] `https://github.com/italia/covid19-opendata-vaccini`
[2] `https://github.com/pcm-dpc/COVID-19`

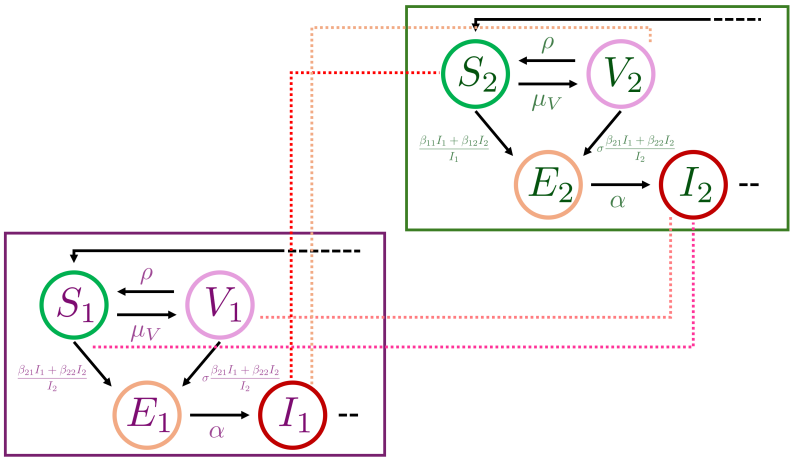

Figure 2: Sketch of the SEIHRV model in a single exposure context and two ages group.

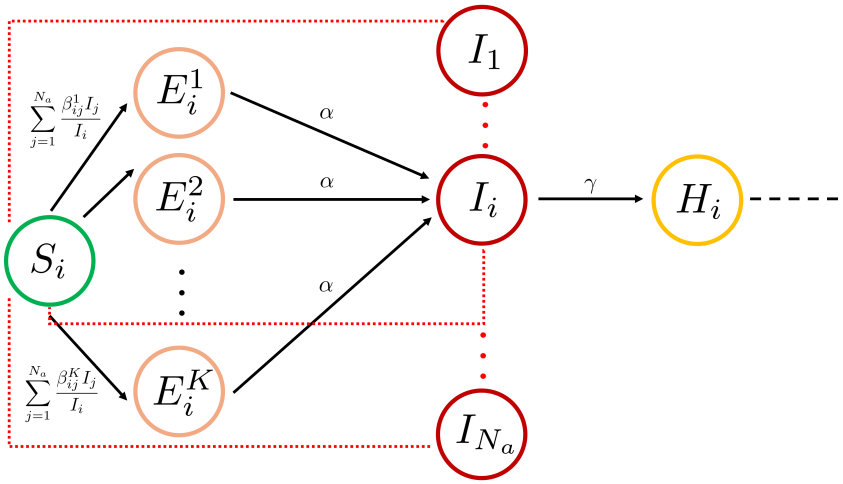

Figure 3: Interactions among the compartments in SEIHRDV multi-age and multi-group model, with $K = 7$ contexts of exposition and $N_a = 15$ age groups.

2.2 The multi-age and multi-context SEIHRDV model

In this section we present the SEIHRDV model. We consider:

- $N_a = 15$ age groups, by assigning to each of the following age groups the corresponding SEIHRDV variables: $\{0 \div 4, 5 \div 9, 10 \div 14, 15 \div 19, 20 \div 24, 25 \div 29, 30 \div 34, 35 \div 39, 40 \div 44, 45 \div 49, 50 \div 54, 55 \div 59, 60 \div 64, 65 \div 69, 70+\}$;
- $K = 7$ contexts of exposition: family, home, school, work, transport, leisure and others.

The interactions among the compartments of the various age groups ([40]) in the different exposure context are sketched in Figure 2. For the sake of simplicity, we limit ourselves to two age groups, named *group 1* and *group 2*, and only one exposure context for each age group. The corresponding compartments are denoted with S_i, E_i, I_i, H_i, R_i, D_i, and V_i, with $i \in 1, 2$. The disease spreads as far as an individual from S_1 can have a contact with either an infectious individual from the same age group, I_1, or an individual

from I_2. Therefore the transmission rate β of the virus is replaced by the expression $\dfrac{\beta_{11}\, I_1 + \beta_{12}\, I_2}{I_1}$, that takes into account both the possible contacts. The same holds for an individual in S_2 with the appropriate modifications.

Extending this argument for all the $N_a = 15$ age groups, and considering the $K = 7$ contexts of exposition, we obtain the complete SEIHRDV multi-age and multi-group model (Figure 3): an individual of age group i can have contacts with infectious individuals belonging to the N_a age groups in the K contexts of exposition. In particular, we denote with E_i^k the number of individuals in age group i who become exposed in the context k, and with β_{ij}^k the transmission rate of I_j in contact with S_i in the context of exposition k. In the multi-age and multi-context SEIHRDV, β can be seen as a third order tensor with components β_{ij}^k.

The equations describing the multi-age and multi-context model read as:

$$
\begin{aligned}
&\frac{dS_i}{dt} = -\left(\sum_{k=1}^{K}\left(\sum_{j=1}^{N_a} c\,\beta_{ij}^k I_j\right)\right)\frac{S_i}{N_i} - d_i\,\frac{S_i}{S_i+R_i} + \mu_R\, R_i + \mu_V\, V_i,\\
&\frac{dE_i^k}{dt} = \left(\sum_{j=1}^{N_a} c\,\beta_{ij}^k I_j\right)\frac{(S_i + \sigma\, V_i)}{N_i} - \alpha\, E_i^k,\\
&\frac{dI_i}{dt} = \alpha\left(\sum_{k=1}^{K} E_i^k\right) - \gamma I_i, \qquad\qquad k = 1,\dots,K,\\
&\frac{dH_i}{dt} = \gamma I_i - \omega H_i, \qquad\qquad t \in (0,T]\\
&\frac{dR_i}{dt} = (1 - f(S_i,V_i))\omega H_i - \mu_R R_i,\\
&\frac{dD_i}{dt} = f(S_i,V_i)\omega H_i,\\
&\frac{dV_i}{dt} = -\left(\sum_{k=1}^{K}\left(\sum_{j=1}^{N_a} c\beta_{ij}^k I_j\right)\right)\frac{\sigma V_i}{N_i} + d_i\frac{S_i}{S_i+R_i} - \mu_V V_i,\\
&S_i(0) = S_{i_0}, \quad E_i^k(0) = E_{i0}^k, \quad I_i(0) = I_{i_0}, \quad H_i(0) = H_{i_0}, \quad R_i(0) = R_{i_0}, \quad D_i(0) = D_{i_0}, \quad V_i(0) = V_{i_0}\\
&\forall\ i = 1,...,N_a.
\end{aligned}
\tag{3}
$$

2.3 Tables of contacts and $\boldsymbol{\beta}-$ matrices

To estimate the transmissibility rate β for different age-groups in different exposure contexts, we use the tables of contacts, based on those proposed by the POLYMOD study [30]. The social contact matrices reported in [30] for different countries estimate the average number of contacts that individuals from an age group have in the following contexts: home, school, work, transport, leisure and other. In particular, we use the table referring to the Italian case that was also considered by the Italian Scientific Technical Committee (CTS) in the early phase of the COVID-19 epidemics (see [41]). The CTS was established in Italy on February 2020 to provide advice and support for coordination activities to overcome the epidemiological emergency due to the spread of the Coronavirus; see also [42]. In addition to the 5 exposure contexts outside the household, as outlined in [30], we account for a total of $K = 7$ distinct exposure contexts. Specifically, based on data from the Italian National Statistics Institute (ISTAT) regarding population and household composition, we disaggregate household contacts into two categories: those occurring exclusively among family members (*"family"*) and those involving both family and non-family members (*"home"*). This distinction enables the consideration of different restrictions implemented in Italy during short periods in 2021. Notably, in specific administrative regions, visits to family members were occasionally prohibited.. The actual social contact matrix used in the present work is reported in Table 1.

		Exposure context						
Ages	**Tot**	**Family**	**Home**	**School**	**Work**	**Transport**	**Leisure**	**Other**
0÷4	16.54	2.30	2.19	5.27	0.00	0.98	3.06	2.75
5÷9	20.49	2.27	2.34	8.87	0.00	1.12	4.53	1.37
10÷14	27.38	2.21	2.22	11.98	0.20	1.35	5.62	3.80
15÷19	29.28	2.05	2.54	13.22	0.05	1.74	6.83	2.87
20÷24	22.15	1.49	2.02	1.17	4.49	0.96	7.23	4.80
25÷29	21.00	1.04	2.43	2.23	5.21	1.13	6.30	2.66
30÷34	18.03	1.26	2.29	0.85	3.92	0.76	5.24	3.72
35÷39	21.25	1.75	2.63	0.68	7.78	1.05	3.92	3.45
40÷44	22.35	1.63	2.25	2.53	7.00	0.67	4.48	3.79
45÷49	19.27	1.50	1.49	2.61	8.24	0.88	1.93	2.64
50÷54	22.30	1.38	1.37	5.54	8.05	0.52	2.02	3.41
55÷59	18.27	1.11	1.77	1.41	4.60	0.68	3.62	5.06
60÷64	18.43	0.91	2.37	1.07	6.05	0.87	3.53	3.63
65÷69	12.74	0.71	2.39	0.55	0.48	0.95	3.33	4.33
70+	10.55	0.71	2.53	0.06	1.04	0.22	4.22	1.77

Table 1: Average number of contacts by age groups, total and disaggregated by social context in which the contact takes place, adding "family" context.

Age groups	0÷4	5÷9	10÷14	15÷19	20÷24	25÷29	30÷34	35÷39
risk$_A$	0.34	0.34	0.34	1	1	1	1	1
Age groups	40÷44	45÷49	50÷54	55÷59	60÷64	65÷69	70+	
risk$_A$	1	1	1	1	1	1.47	1.47	

Table 2: Susceptibility by age group

Level of the risk	Low	Medium-Low	Medium	Medium-High	High	Very High
risk$_E$	0.25	0.5	1	1.5	2	2.5

Table 3: Levels of risk associated to the contexts of exposition

On the basis of the social contact data provided in [30], it is possible to estimate, for each context of exposition, the daily contacts of each individual distributed in the different age groups (cf. Figure 4), as well as the total number of daily contacts that each individual of a given age group has with individuals in different age groups and in different contexts of exposition (cf. Figure 5).

These contact matrices have been used to determine the $\beta - matrices$ that express the transmissibility rate for each age class in each exposure contexts. However, the number of contacts is not the only factor that should be taken into account. Indeed, as suggested in [41], age-dependent susceptibility to the infection should also be considered, that we denote $risk_A$ (Table 2), as well as different levels of risk to contract the virus in the different contexts of exposition [43], denoted as $risk_E$ (Table 3).

The risk associated to each age group is based on a CTS report, [41], which states that children under 14 have a 66% lower than average risk of contract the infection, while adults over the age of 65 have a 47% above average risk of infection. On the other hand, the risk factor associated with each exposure context depends on the relative contribution of the various sectors (sub-contexts) that constitute it. Specifically, we assign a risk level to each sector by considering four key factors: the presence of closed spaces, the duration of interactions, the density of the crowd, and activities involving forced exhalation (such as sneezing, yelling, singing, and coughing). For the following contexts of exposition, we consider different sectors as follow:

- **school context**: it is split into six sectors (nursery, kindergarten, elementary school, middle school,

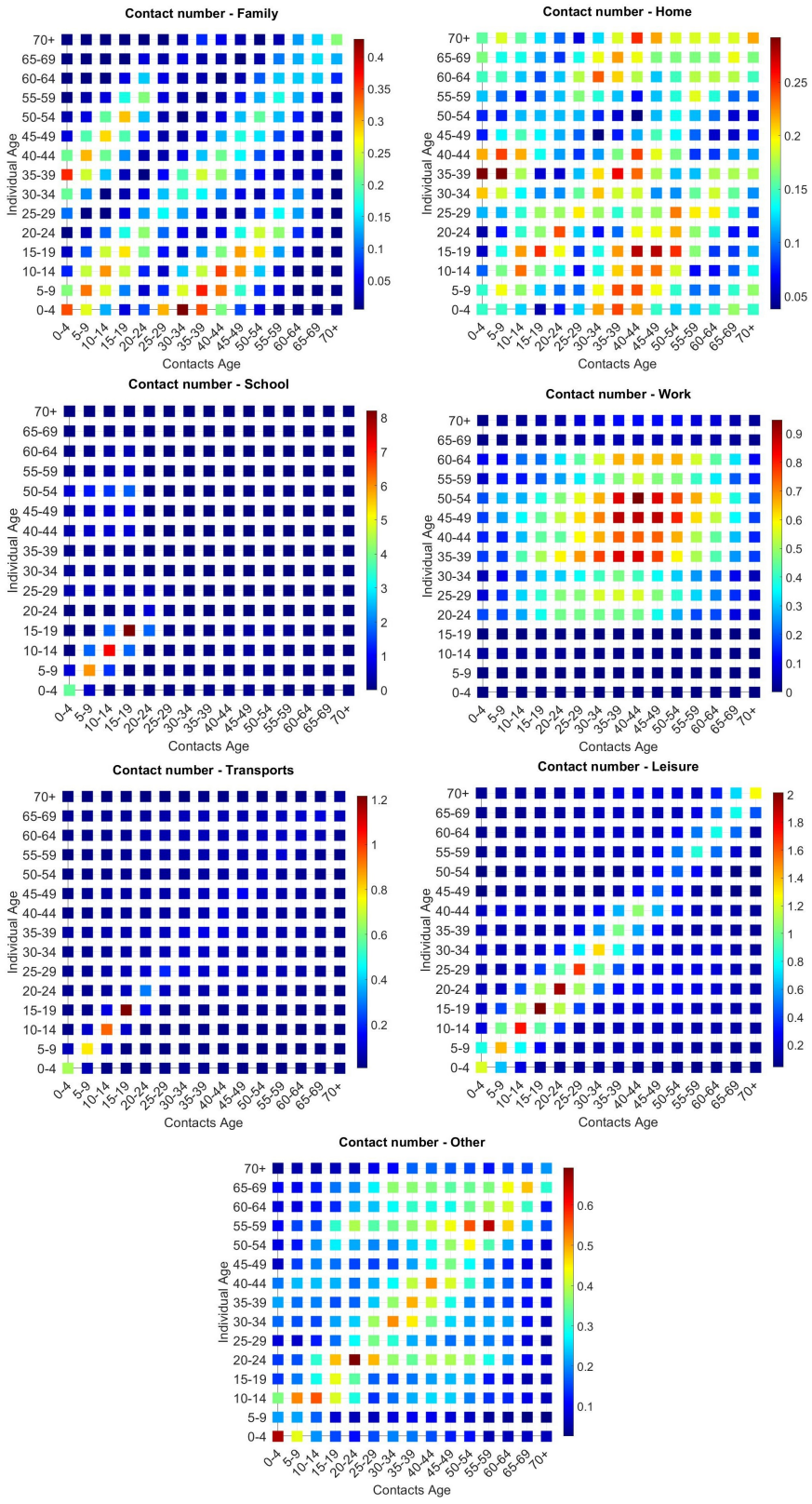

Figure 4: POLYMOD matrices $M^k_{i,j}$, $k = 1, ..., 7 = K$, $i, j = 1, ..., 15 = N_a$: total number of contacts that each individual has with individuals from the 15 age groups, in the seven contexts of exposition.

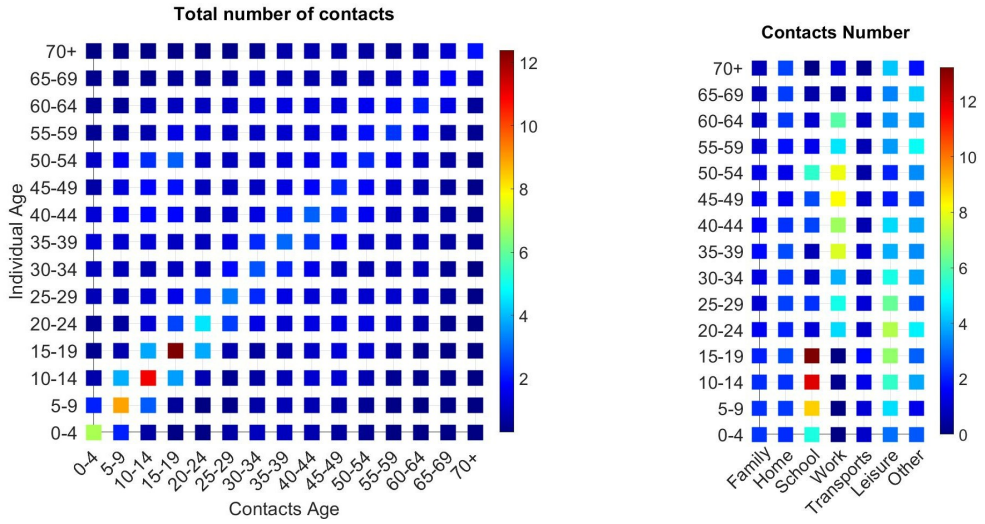

Figure 5: Total number of contacts that each individual has with individuals from the 15 age groups at left, for each exposure context at right.

high school and university);

- **work context**: it is divided into seven sectors (essential, healthcare, manufacturing, trade, construction, restaurant/hotel, other);
- **leisure context**: is divided into six sectors (outdoor restaurants, indoor restaurants, outdoor pub/disco, indoor pub/disco, indoor sport, outdoor sport);
- **"other" context**: is divided into three sectors (essential retail, other not essential retail, mass and religious events).

The home context takes into account contacts that occur in households, but not among co-habitants, which are instead referred to the family context. No split is considered for the transport context.

Then, a scenario can be defined by assigning values in $[0, 1]$ for each sector of the various contexts, to indicate their opening/closing considered according to the regulations in force (0 if the sector is totally closed, 1 if it is totally opened, values in $(0, 1)$ if there are other restrictions). To obtain the $\beta - matrix$ that expresses the effective risk of transmission for each age group in contact with other age groups in the different contexts of exposition, we multiply the k-th contact matrix by a function depending on the risk parameters defined above and on the chosen scenario, which expresses the level of opening/closure of the sub-contexts:

$$\beta^k_{i,j} = M^k_{i,j}\ h_k(risk^{S_k}_E, risk_A, scenario^l_k) \quad \text{for all sectors } l = 1, \dots, S_k, \quad \text{for all context } k = 1, \dots, K, \quad (4)$$

where i is the age of the individual, j is the age of the contact, M^k is the contact matrix of the context k, S_k is the number of sectors of the k^{th} context of exposition and h_k is a piecewise constant context-dependent function, in which for each age group we calculate a value expressing the global risk associated to the specific context k. The latter function depends on:

- $risk^{S_k}_E$, that is the value of risk assigned to each of the S_k sectors of the context k between low, medium-low, medium, medium-high, high and very high risk (Table 3);
- $risk_{Ai}$, that is the vector containing the risk for each age group (Table 2);

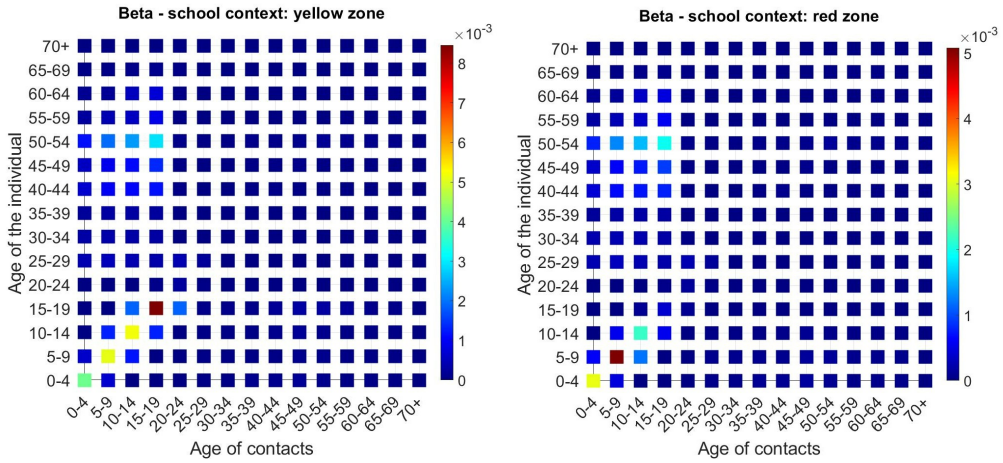

Figure 6: $\beta - matrices$ in school context, for yellow zone scenario at left, for red zone scenario at right.

- $scenario_k^l$, that is the level of opening/closing (in $[0, 1]$) of each sector l of the exposure context k, as we defined before.

Starting from November 2020, in Italy, containment measures differentiated by region are introduced, due to the fact that the spread of the virus was different on the peninsula. This differentiation is expressed in colors: *yellow* for the regions with a transmissibility index less than 1.25, *orange* for regions with transmissibility index between 1.25 and 1.5, where the associated NPIs have more restrictions, and *red* for regions with transmissibility index greater than 1.5. The NPIs associated to red regions are the more restrictive, corresponding to almost complete lockdowns. These measures are issued with an order from the Minister of Health, in agreement with the president of the region concerned and the CTS, and must have a minimum duration of 15 days, since their impact on the transmission mechanism is delayed, as estimated, e.g., in [44]. The conditions for the regions to switch the associated color have changed during the evolution of the pandemic, and *white* zones have been also introduced in January 2021, corresponding to the almost complete dismissal of mobility restrictions.

In Figure 6 we can see the $\beta - matrices$ of school context associated to two different scenarios: yellow zone and red zone. In yellow zone the restrictions included schools totally open up to the third year of middle school and high schools open to 50%, while in red zone we had schools open up to the first year of middle school, while second and third year of middle school, high schools and universities were totally closed.

With different containment measures in force for each region, to define the scenario we have to make different considerations depending on whether we are simulating on a national or regional basis. At regional level it is sufficient to reconstruct the temporal history of the regional restrictions, instead at national level it is necessary to take into account the different containment measures in force in each region, and to reconstructed an average measure for the restrictions. To do that, for each week, we analyzed the regional restrictions in force (which regions where in yellow zone, which in orange, which in red, which in white zone), and we set the final scenario weighing all these different scenarios on the population of each region. In fact regions with small populations have less weight on Italian situation than large regions.

In the national case, we consider an array $\mathbf{n}$ in which each component corresponds to the number of inhabitants of an Italian region. Moreover, we consider arrays for each color zone (for example red zone, orange zone, yellow zone and green zone) having one entry for each region, in which we have 1 if the corresponding region (in the same order of the previous array) has government restriction of that color, 0 if there are other color restriction. For example, calling $\mathbf{r}$ the array of binary values corresponding to red zone, $\mathbf{o}$ the respective array for the orange zone, $\mathbf{y}$ for the yellow zone and $\mathbf{w}$ for the white one. Multiplying the inhabitants array $\mathbf{n}$ with each color zone array we obtain the number of the Italian population under that

color zone restriction:

$$r_n = \sum_{i=1}^{N} \mathbf{r}_i \mathbf{n}_i, \qquad o_n = \sum_{i=1}^{N} \mathbf{o}_i \mathbf{n}_i, \qquad y_n = \sum_{i=1}^{N} \mathbf{y}_i \mathbf{n}_i, \qquad \text{and} \qquad w_n = \sum_{i=1}^{N} \mathbf{w}_i \mathbf{n}_i,$$

where r_n is the number of Italian people in red Zone restrictions, o_n is the number of Italian people in orange zone restrictions, y_n is the number of Italian people in yellow zone restrictions and w_n is the number of Italian people in White Zone restrictions.

Finally, we derive the national scenario by averaging as follows:

$$scenario_k^l = \frac{r_n s_{r_k}^l + o_n s_{o_k}^l + y_n s_{y_k}^l + w_n s_{w_k}^l}{r_n + o_n + y_n + w_n}, \qquad l \in 1, ..., S_k, \quad k \in 1, ..., K$$

where $scenario_k^l$ is the value in $[0, 1]$ assigned to the l^{th} sector of the k^{th} context of exposition of the scenario, $s_{r_k}^l$. Instead, $s_{o_k}^l$, $s_{y_k}^l$ and $s_{w_k}^l$ are the values in $[0, 1]$ assigned to the l^{th} sector of the k^{th} context of exposition of the red zone scenario, the orange zone scenario, the yellow zone scenario and the white zone scenario respectively.

2.4 Data generation and calibration of the parameters

In this section, we describe the calibration procedure (see Section 2.4.1) for determining model parameters that could not be directly derived from clinical or population cohort studies. Furthermore, we detail the processing of vaccination data (cf. Section 2.4.2) and describe the adjustments made to the model to incorporate the social restrictions introduced under the *Green Pass* initiative (cf. Section 2.4.3).

2.4.1 Calibration

Model calibration poses significant challenges in epidemic modeling, as inaccurate reconstructions can critically compromise the quality of scenario analyses and forecasts. Special attention must be given to parameters governing the transmission mechanism, particularly the function $c(t)$ in our model, as it plays a pivotal role in determining the model's reliability [26].

For this purpose, we undergo a Least-Square calibration procedure based on reported deceased data from Dipartimento di Protezione Civile Italiana (DPC). Indeed, the compartment of deceased individuals is the only one with a direct counterpart in DPC data and is generally the least affected by monitoring uncertainties. In our cases, both $c(t)$ and $\beta(t)$ (cf. Section 2.1) are piecewise constant functions. The values of $c(t) = \sum_{i}^{N_{int}} c_i I_{(t_i, t_{i+1}]}(t)$ are calibrated separately for each time subinterval corresponding to a specific scenario (e.g., a particular restriction level). The iterative calibration stage is carried out according to the following steps:

1. Associate a $\beta - matrix$ for each subinterval corresponding to the prescribed scenario;
2. Solve the following optimization problem:

$$\min_{\{c_i\}_i} J(c) = \sum_{t=0}^{T} \frac{(D(t) - \hat{D}(t))^2}{\left(\hat{D}(t)\right)^2}, \tag{5}$$

where $\hat{D}$ is the total number of deceased individuals provided by the DPC in [0,T]

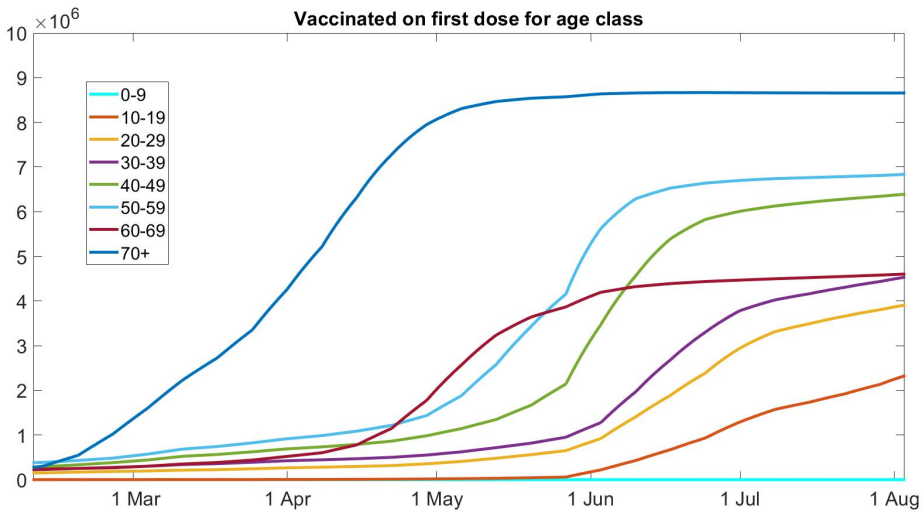

Figure 7: Vaccinated in first dose for DPC age groups.

2.4.2 Vaccination campaign

The Italian COVID-19 vaccination campaign included the administration of two doses and a booster (third) dose in the late periods of the outbreak. These dynamics are incorporated into our model using vaccination data provided by DPC, enabling us to track the participation of individuals in the vaccination campaign. At the beginning of the vaccination campaign, vaccinations were initially delivered by age group. In particular, these data are split into eight age groups $\{0 \div 9, 10 \div 19, 20 \div 29, 30 \div 39, 40 \div 49, 50 \div 59, 60 \div 69, 70+\}$, even though in our model we consider fifteen age groups $\{0 \div 4, 5 \div 9, 10 \div 14, 15 \div 19, 20 \div 24, 25 \div 29, 30 \div 34, 35 \div 39, 40 \div 44, 45 \div 49, 50 \div 54, 55 \div 59, 60 \div 64, 65 \div 69, 70+\}$. Thus, to initialize our model we make the following assumption: calling A_i the age groups provided by data, with $i = 1, ..., 8$, and B_j the age groups used in our model, with $j = 1, ..., 15$, the number of the initial vaccinated individuals of the age groups B_j is given by

$$|B_j| = \frac{|A_k|}{2}, \quad j = 1, \ldots, 14,$$

where

$$k = \begin{cases} \left\lfloor \frac{j}{2} \right\rfloor + 1 & \text{if} \quad j \mod 2 = 1 \\ \left\lfloor \frac{j}{2} \right\rfloor & \text{if} \quad j \mod 2 = 0 \end{cases} \tag{6}$$

and $|B_{15}| = |A_8|$. In this way, we are able to exploit the SEIHRDV multi-age and multi-group for reproducing the curve of vaccinated people evolving over time for each age group. In Figure 7 we report this evolution in the 8 DPC age-classes, finding agreement with the actual administrations *per-age*.

In our model, we explicitly include only individuals vaccinated with at least one dose in the compartment V. The efficacy parameter σ, as estimated from clinical trials [28], was an appropriate choice when the number of individuals with only the first dose surpassed that of fully vaccinated individuals. However, by late 2021, approximately 78% of the Italian population had received at least one dose, with nearly 74% fully vaccinated. Furthermore, vaccine effectiveness in reducing COVID-19 transmissibility is estimated to decline approximately six months after full vaccination, necessitating the introduction of the third, or booster, dose. Consequently, for these later periods, we compute σ as a weighted parameter, determined as follows:

$$\sigma(t) = \frac{\sigma_1 V_{D_1}(t) + \sigma_2 \left(V_{D_2}(t) + V_{D_4}(t)\right) + \sigma_3 V_{D_3}(t)}{V_{D_1}(t) + V_{D_2}(t) + V_{D_3}(t) + V_{D_4}(t)}, \tag{7}$$

with

- σ_1, rate of ineffectiveness in reducing virus transmissibility for those who received only the first dose of the vaccine;
- σ_2, rate of ineffectiveness in reducing virus transmissibility for those who have been fully vaccinated (double dose of vaccine) for less than six months;
- σ_3, rate of ineffectiveness in reducing virus transmissibility for those who have been fully vaccinated (double dose of vaccine) for more than six months;
- $V_{D_1}(t)$ number of individuals who received only the first dose of vaccine on day t (DPC);
- $V_{D_2}(t)$ number of individuals who are fully vaccinated (with two doses) for less than six months on day t (DPC);
- $V_{D_3}(t)$ number of individuals who are fully vaccinated (with two doses) for more than six months on day t (DPC);
- $V_{D_4}(t)$ number of individuals who are vaccinated with the booster dose on day t (DPC).

We assume that individuals receiving the booster dose regain the vaccine efficacy that achieved in the first few months after full vaccination. In our model we do not distinguish on the various vaccines used, hence the ineffectiveness values are estimated from average values of different vaccines data collected in the literature. In particular we estimate $\sigma_{\mathbf{1}} = 0.30$, $\sigma_{\mathbf{2}} = 0.12$ and $\sigma_{\mathbf{3}} = 0.50$.

Finally, to determine the value of θ, introduced in the model in (2), we utilize data from the ISS as reported in [45]. Specifically, we analyze the ratio of unvaccinated individuals who died relative to unvaccinated COVID-19 diagnoses and the ratio of vaccinated individuals who died relative to vaccinated COVID-19 diagnoses. From this analysis, we set $\theta = 0.8$, which implies that for vaccinated individuals diagnosed with COVID-19, the vaccine reduces mortality by 20%.

2.4.3 Green Pass

On June 17, 2021, Italy introduced the Green Pass restriction for the first time. The Green Pass, a digital COVID certificate proposed by the European Commission, aimed to facilitate the safe and unrestricted movement of European Union citizens during the COVID-19 pandemic. In Italy, the Green Pass certified one of the following conditions: receipt of a COVID-19 vaccination (issued after each vaccine dose), a negative result from a rapid antigen test within the previous 48 hours or a molecular test within the previous 72 hours, or recovery from COVID-19 within the last 6 months.

We modify the model to take into account the restrictions due to the Green Pass. For this purpose, we introduce a second rate of transmissibility, β_S, which expresses the probability that a susceptible individual will contract the virus after a contact with an infectious, considering the limitations due to not having the Green Pass. For simplicity we are considering as Green Pass holders the individuals who have received at least one dose of vaccine. So the individuals in V, which are Green Pass holders, are not subject to the same restrictions. For them, we consider the transmissibility rate β defined earlier. If the Green Pass restrictions

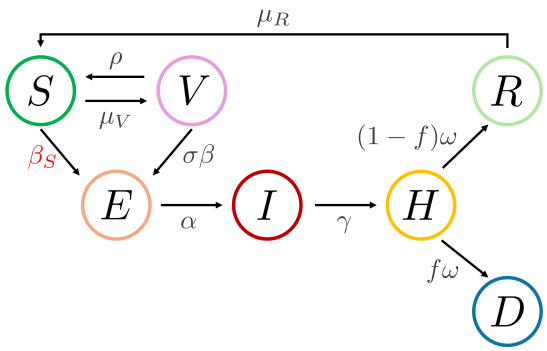

Figure 8: SEIHRDV model adapted to take into account Green Pass restrictions.

were lifted, then $\beta_S = \beta$. Therefore, the equations become:

$$
\begin{aligned}
&\frac{dS_i}{dt} = -\left(\sum_{k=1}^{K}\left(\sum_{j=1}^{M} c(t)\,\beta_S {}^{k}_{ij} I_j\right)\right)\frac{S_i}{N_i} - d_i\,\frac{S_i}{S_i+R_i} + \mu_R\,R_i + \mu_V\,V_i,\\
&\frac{dE_i^k}{dt} = \left(\sum_{j=1}^{M} c(t)\,\beta_S {}^{k}_{ij}\,I_j\right)\frac{S_i}{N_i} + \left(\sum_{j=1}^{M} c(t)\,\beta_{ij}^{k}\,I_j\right)\frac{\sigma\,V_i}{N_i} - \alpha\,E_i^k, \qquad k = 1,\dots,K,\\
&\frac{dI_i}{dt} = \alpha\left(\sum_{k=1}^{K} E_i^k\right) - \gamma\,I_i,\\
&\frac{dH_i}{dt} = \gamma\,I_i - \omega\,H_i, \qquad t \in (0,T],\\
&\frac{dR_i}{dt} = (1 - f(S_i,V_i))\,\omega\,H_i - \mu_R\,R_i,\\
&\frac{dD_i}{dt} = f(S_i,V_i)\,\omega\,H_i,\\
&\frac{dV_i}{dt} = -\left(\sum_{k=1}^{K}\left(\sum_{j=1}^{M} c(t)\,\beta_{ij}^{k}\,I_j\right)\right)\frac{\sigma\,V_i}{N_i} + d_i\,\frac{S_i}{S_i+R_i} - \mu_V\,V_i,\\
&S_i(0) = S_{i_0}, \quad E_i^k(0) = E_{i_0}^k, \quad I_i(0) = I_{i_0}, \quad H_i(0) = H_{i_0}, \quad R_i(0) = R_{i_0}, \quad D_i(0) = D_{i_0}, \quad V_i(0) = V_{i_0},\\
&\forall i = 1,...,N_a.
\end{aligned}
\tag{8}
$$

3 Results

We report numerical results obtained in different scenarios for both the global and regional Italian levels. Our aim is to capture how the COVID-19 developed in the different contexts of exposition among the different age-groups and to assess the validity of the proposed novel compartmental model. For each period selected, an accurate research was carried out to set the scenario parameters, taking into account the containment measures in force and their variations in the respective time-frame.

In particular, in Section 3.1 we present the results set at the Italian national level from September 2020 to July 2021, in Section 3.2 we analyze the same period in Lombardy and Lazio, whilst in Section 3.3 we report the results for the whole Country up to December 2021, in order to evaluate the impact of the Green Pass measure.

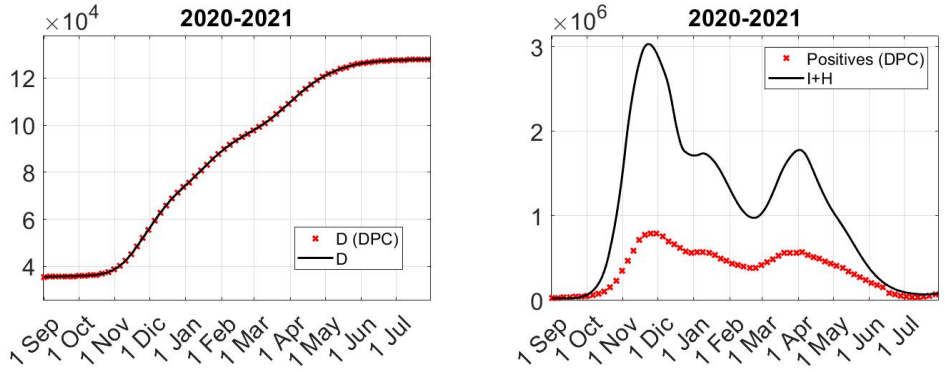

Figure 9: Calibration results in Italy: the calibration on reported deceased (left), the sum of Infectious and Healing estimated by the model compared with reported positives (right).

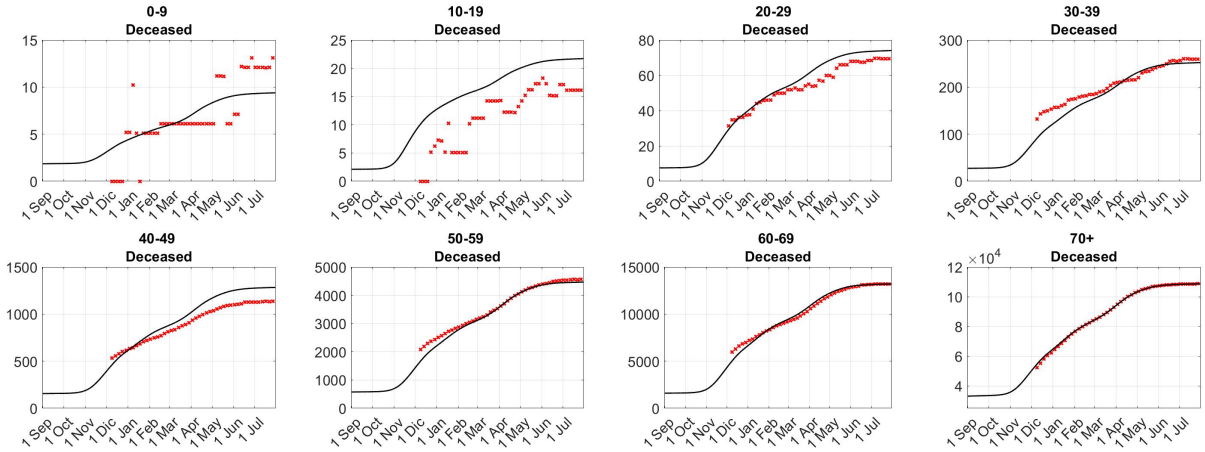

Figure 10: Deceased in Italy from September 2020 to July 2021 estimated by SEIHRDV multi-age and multi-context model divided by age group, compared with data (in red).

3.1 September 2020 - July 2021: Italy

At the beginning of the period of interest very few NPI restrictions were in force, and in particular schools were open. With the increase in infections, regional restrictions were introduced starting from November, with the classification in 3 colors according to the risk: yellow, orange and red.

For the first calibration we set $\theta = 1$ and $\mu_R = 0$, so we consider that, once the positive diagnosis is received, vaccines are totally ineffective in reducing deaths, and that recovered individuals become immune. Note that if we consider $\theta = 1$, the function $f(S, V; \tau)$ defined in (2) is equal to the *Infectious Fatality Rate*.

As we can see in Figure 9, the amount of deceased matches with actual monitoring, showing a reasonable behavior of the curve of positive individuals. Indeed, it is possible to see that $I + H$ curve follows the trend of the positives given by DPC. The gap between the two curves is due to monitoring uncertainty: SEIHRDV model does not distinguish detected from undetected individuals.

In Figure 10 we compare deceased individual divided by age groups, since we are able to reconstruct the IFR for each age class. Even in this case, the stratification of deceased matches with available data. In Figure 11 the curves of positives individuals (i.e. Infectious and Healing individuals) estimated by SEIHRDV multi-age and multi-context model follow the trend of the data. As in Figure 9, the gap between the curves and the data is motivated by the limitations in monitoring. In particular, in the 70+ age group we observe that estimated curve and data are similar: this is probably due to the fact that older individuals are more

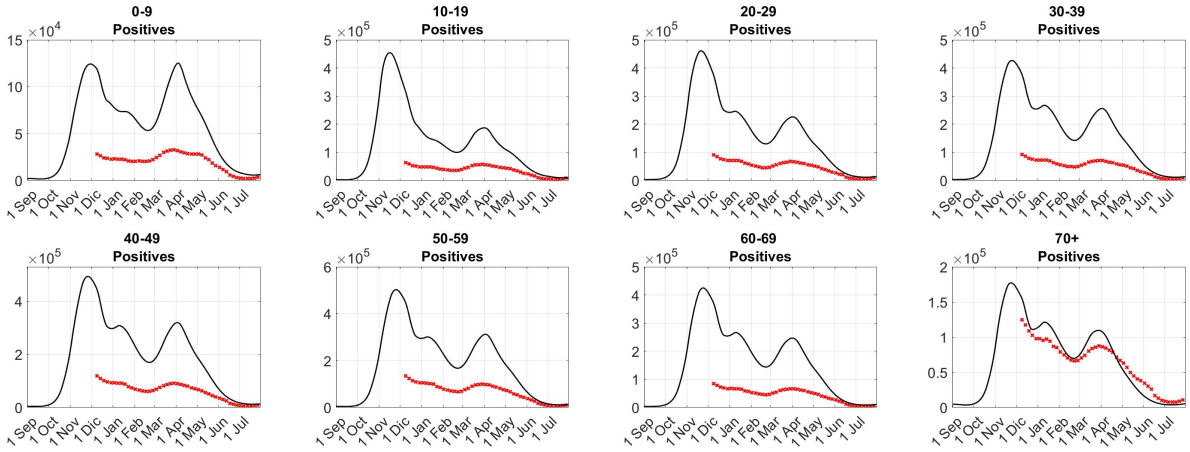

Figure 11: Positives ($I + H$) in Italy from September 2020 to July 2021 estimated by SEIHRDV multi-age and multi-context model divided by age group, compared with data (in red).

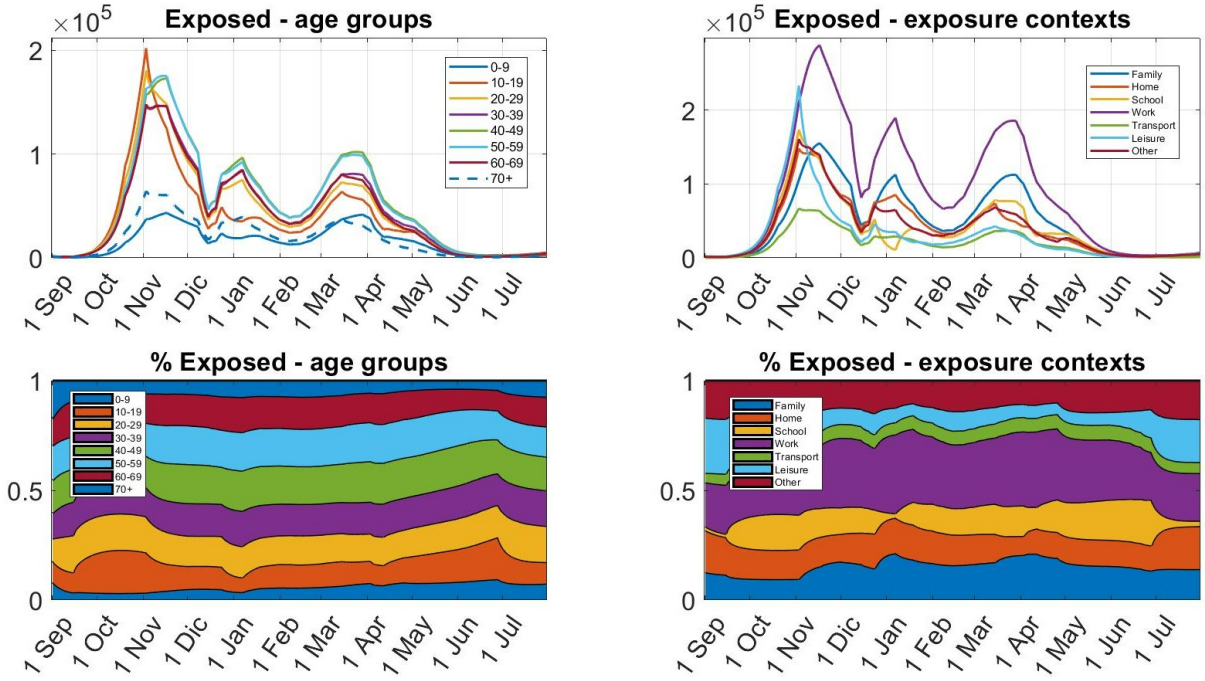

Figure 12: Exposed in Italy from September 2020 to July 2021: at the top, evolution of the exposed individuals divided by age group (a) and context of exposition (b); at the bottom, distribution of age groups (c) and contexts of exposition (d) in the exposed compartment.

often symptomatic than other age groups, and thus they are more easily detected.

The peculiarity of the SEIHRDV multi-age and multi-context is that we can observe how exposed individuals are distributed in each age group and context of exposition. In Figure 12 we show the age-repartition (a) and contexts of exposition (b) of exposed individuals, while at the bottom we have the distribution of age groups (c) and context of exposition (d) in the exposed compartment. In this way, we can interpret the

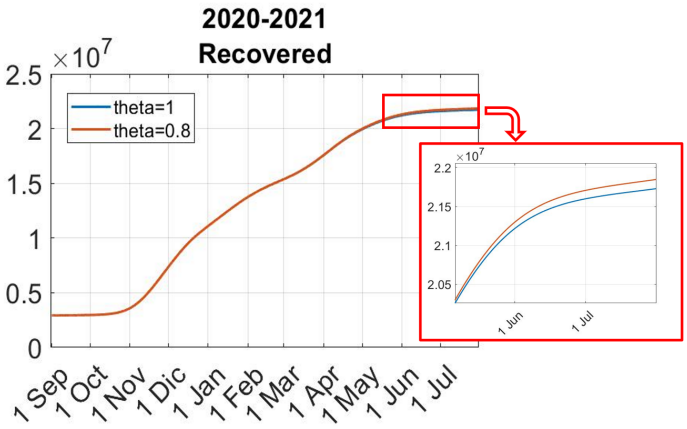

Figure 13: Curves of Recovered with $\theta = 1$ and $\theta = 0.8$ compared in the whole time period.

numerical results in light of the specific NPIs placed in act and evaluate the impact of specific interventions. For instance, in the middle of September 2020 schools were totally open. This led to an increase of cases in the younger age groups until the beginning of November, when some restrictions where applied with the introduction of colored zones. Since then, the most exposed age groups were 40-49 and 50-59. For what concerns the contexts of exposition we can see that, in the first part of the growth of the curve, "leisure" was the context with the greatest exposures. Then, with the introduction of the containment measures of November, the context in which most infections occur was the "work" sector. In the same way, the infections in the "school" context, which was growing, began to decline and then remained more or less constant (with an exception for Christmas holiday). School-related restrictions particularly affected part of middle school students and high school students.

For the sake of completeness, we repeated the numerical tests by imposing $\theta = 0.8$. We estimated this value of θ, that is the rate of inefficacy of vaccination in the reduction of death, from ISS data reported in [45]. We obtained similar results. In particular we can see a difference in the Recovered compartment: if individuals die fewer, we will have more recovered (Figure 13).

3.2 September 2020 - July 2021: regions Lombardy and Lazio

The trend of the national epidemic curve is influenced by the trends of the individual regions. In fact, the situation may be different in each region, depending on average age of individuals, daily habits, hospital situation, climatic situation. For this reason, the NPI in the chosen time period are adopted on a regional scale. Hence, we analyzed what happened in two of the most populous Italian region: Lombardy and Lazio. As we did in Section 3.1, we set up the scenario, the initial conditions by imposing $\theta = 1$ and $\mu_R = 0$.

3.2.1 Lombardy

As we can see in Figure 14, the amount of deceased individuals matches with actual data, showing also in Lombardy a reasonable behavior of positive individuals. The $I + H$ curve follows the trend of the positives given by DPC. Even in this case, the gap between the two curves is due to the accuracy of the detection. In Figures 15 and 16 we report deceased individuals and positives individuals divided by age groups.

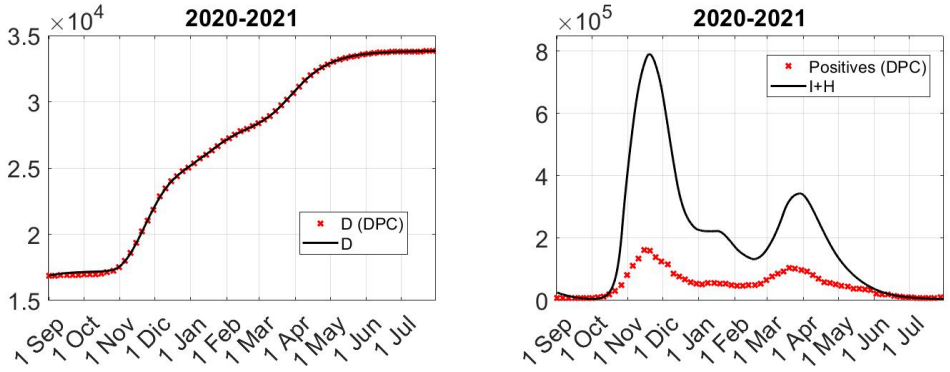

Figure 14: Calibration results in Lombardy: the calibration on reported deceased at the left, the sum of Infectious and Healing estimated by the model compared with reported positives at the right.

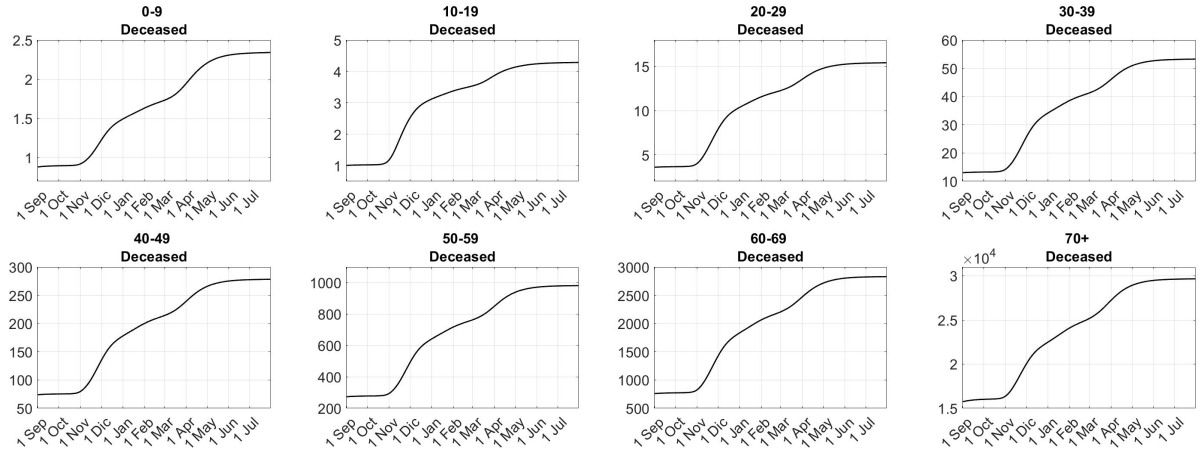

Figure 15: Deceased in Lombardy estimated by SEIHRDV multi-age/multi-context model divided by age group.

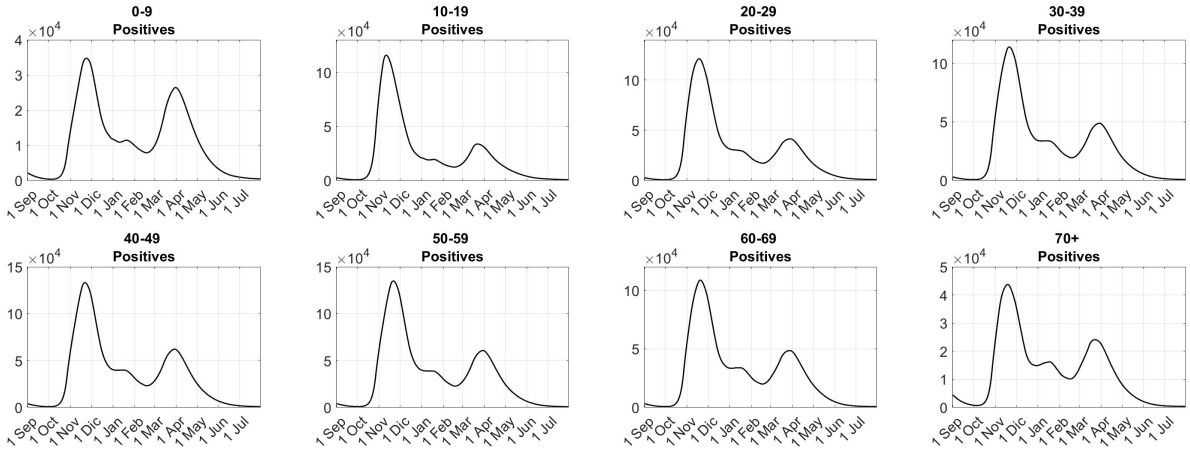

Figure 16: Positives $(I + H)$ in Lombardy estimated by SEIHRDV multi-age/multi-context model divided by age group.

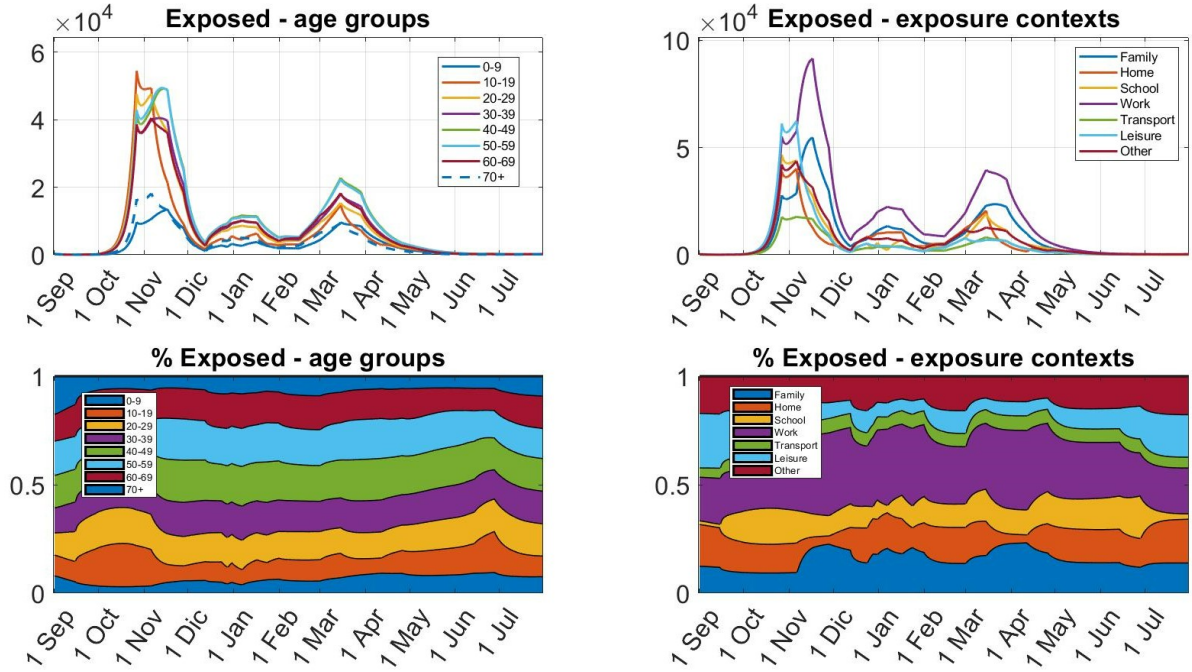

Figure 17: Exposed in Lombardy: at the top, evolution of the exposed individuals divided by age group (a) and context of exposition (b); at the bottom, distribution of age groups (c) and contexts of exposition (d) in the exposed compartment.

With SEIHRDV multi-age and multi-context we are able to track the evolution of infections in each age group and each context of exposition. In Figure 17 we report the amount of exposed divided by age groups and context of exposition, while at the bottom we can see how the exposed (and therefore infections) are divided into age groups and contexts of exposition. As we expected, the curves in Figure 17 follow different trends with respect to the national curve of the exposed individuals (Figure 12).

3.2.2 Lazio

In Figure 18 we observe that even in this case, deceased individuals match the actual data. The curve of positives in the same figure follows the trend of the positives given by DPC, with the usual gap ascribed to monitoring uncertainty. In Figure 19 and 20 we report deceased individuals and positives individuals divided by age groups.

In Figure 21 the amount of exposed is represented divided by age groups and context of exposition, together with how age groups and contexts of exposition are distributed in the exposed compartment. The curves in Figure 21 are different both from the national curves of exposed (Figure 12) and the Lombardy curves (Figure 17).

3.3 September 2020 - December 2021: Italy

In this section, we take into account for the Green Pass restrictions as introduced in Section 2.4.3. To set the scenarios, until the end of July we used the same setting imposed in Section 3.1, while from August onwards we took into account the new rules relating to the Green Pass described below:

- From August 6 to September 12: Green Pass requirement for indoor restaurants, indoor pubs, discos, indoor sports and various events (concerts, museums, cinemas, stadium, shows, theaters);

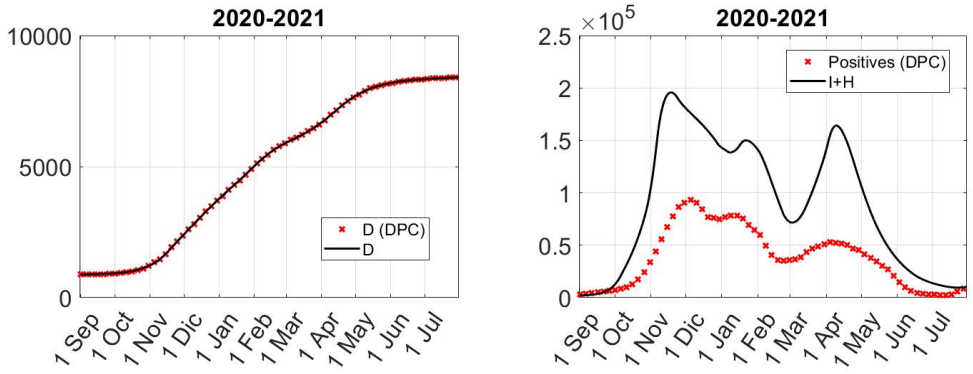

Figure 18: Calibration results in Lazio: the calibration on reported deceased at the left, the sum of Infectious and Healing estimated by the model compared with reported positives at the right.

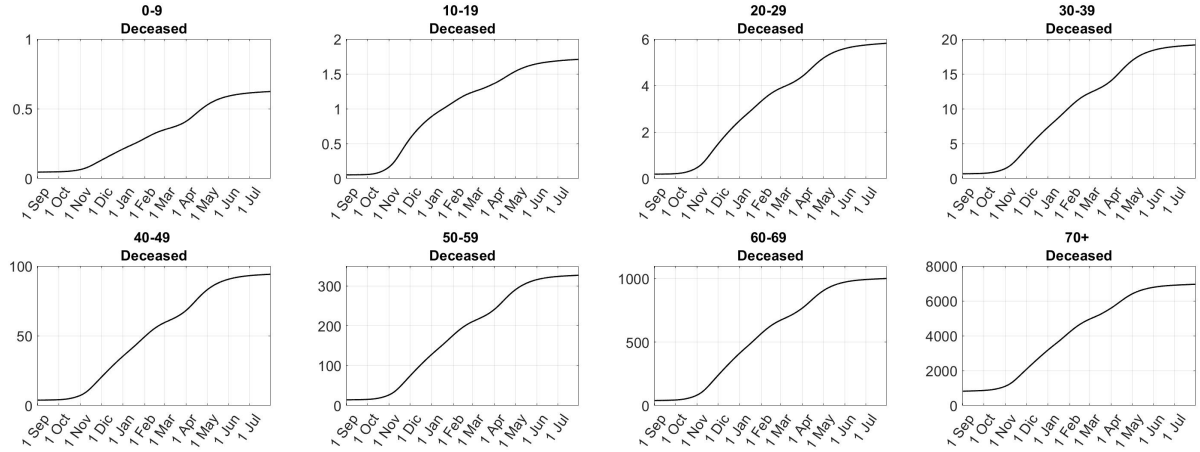

Figure 19: Deceased in Lazio estimated by SEIHRDV multi-age/multi-context model divided by age group.

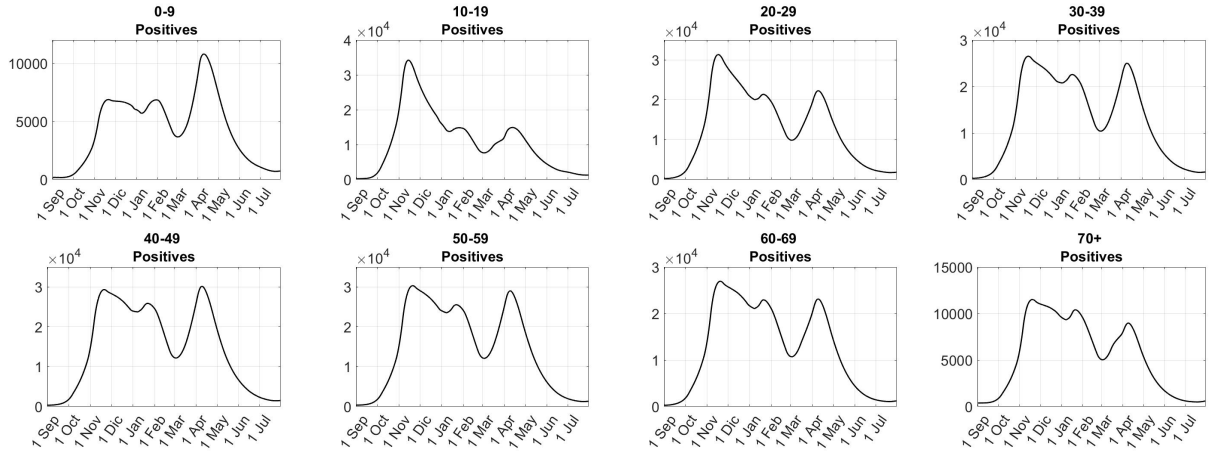

Figure 20: Positives ($I + H$) in Lazio estimated by SEIHRDV multi-age/multi-context model divided by age group.

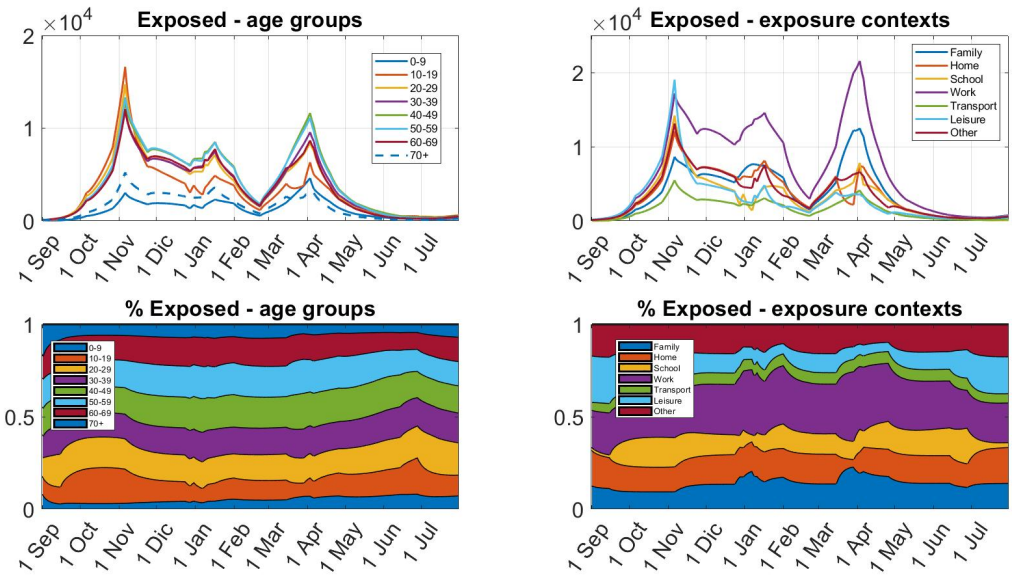

Figure 21: Exposed in Lazio: at the top, evolution of the exposed individuals divided by age group (a) and context of exposition (b); at the bottom, distribution of age groups (c) and contexts of exposition (d) in the exposed compartment.

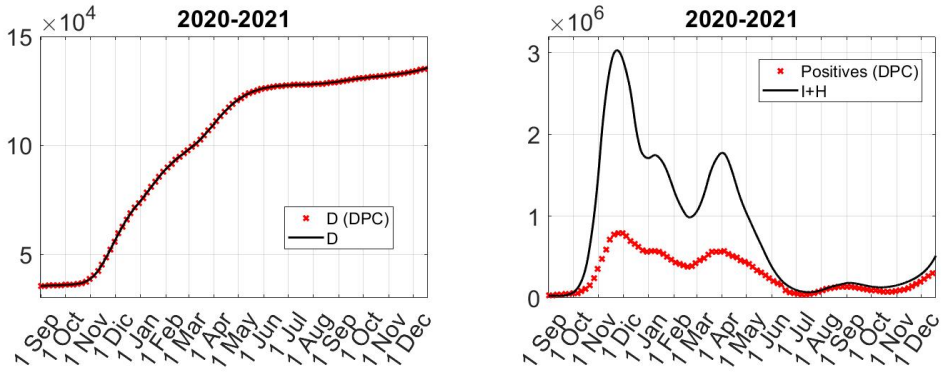

Figure 22: Calibration results in Italy: the calibration on reported deceased at the left, the sum of Infectious and Healing estimated by the model compared with reported positives at the right, introducing GP containment measures.

- From September 13 to October 14: Green Pass requirement also extended to school staff and university students;
- From October 15 onward: Green Pass requirement also extended to workers.

For the sake of simplicity we considered as Green Pass holders only vaccinated individuals, since our model does not explicitly monitor swabs. We consider the same initial condition of the first calibration seen in (3.1), using a non-zero rate of end of immunity for recovered individual since we are considering a time period of over a year.

In Figure 22 we show the trend of positive individuals in the GP case, and observe that it matches available data. Since the gap between the curve and the data is smaller from July, we can deduce that a

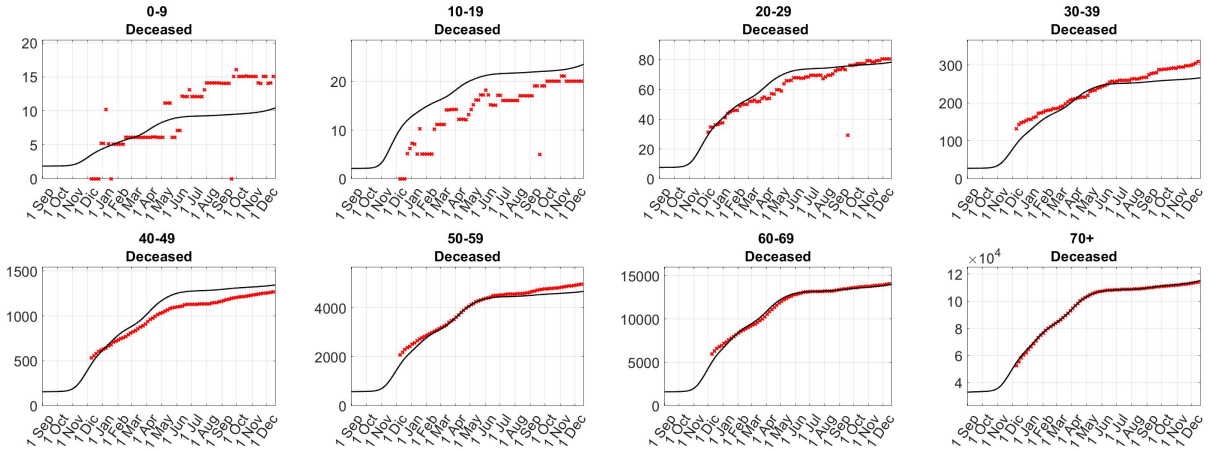

Figure 23: Deceased in Italy estimated by SEIHRDV multi-age/multi-context model divided by age group, introducing GP containment measures.

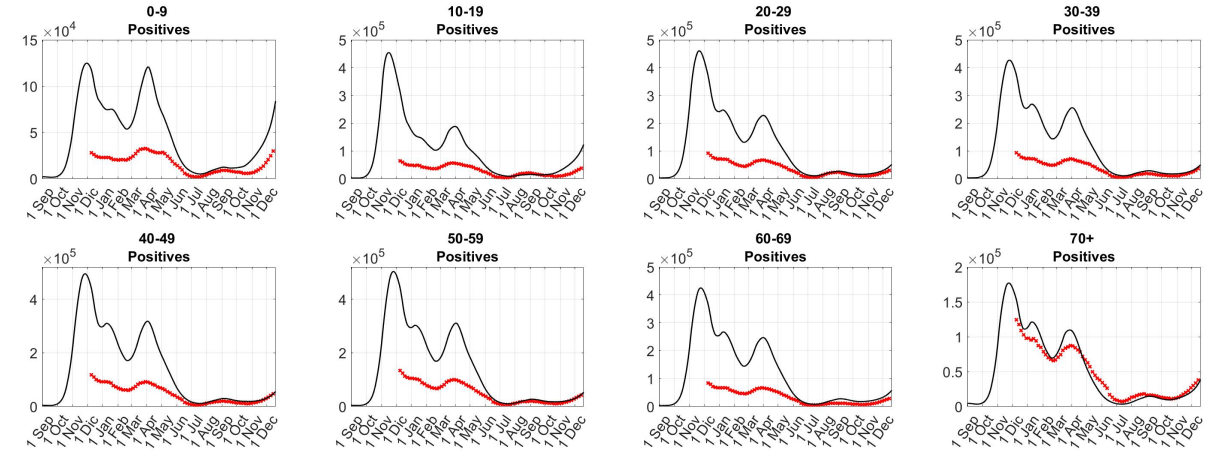

Figure 24: Positives ($I + H$) in Italy estimated by SEIHRDV multi-age/multi-context model divided by age group, introducing GP containment measures.

better monitoring policy is induced by the introduction of Green Pass obligation (notice that the Green Pass can also be granted if swabs are negative). The curve catches also the rise in cases that began in mid-October.

In Figure 24 it is possible to observe differences between the age groups in this last time period. In particular from SEIHRDV multi-age/multi-context model it is possible to see a significant growth in 0-9 and 10-19, maybe due to the school reopening. Indeed in July and August schools were closed, as shown in the distribution of exposed in the different contexts of exposition (Figure 25): starting on September the exposed in "school" context started growing again. In particular, the age groups most affected by school reopening are indeed those aging 0-9 and 10-19 (as can be seen in Figure 25), which are also the ones less vaccinated (the vaccination campaign concerns the over 12s).

Finally, we conclude that the Green Pass NPIs impact more in the context of exposition of *work*, and in a lighter way in *leisure*, as we can see in Figure 25. On the other hand, an increase in the rate of exposure to the virus is observed in contexts such as *school* and *home*.

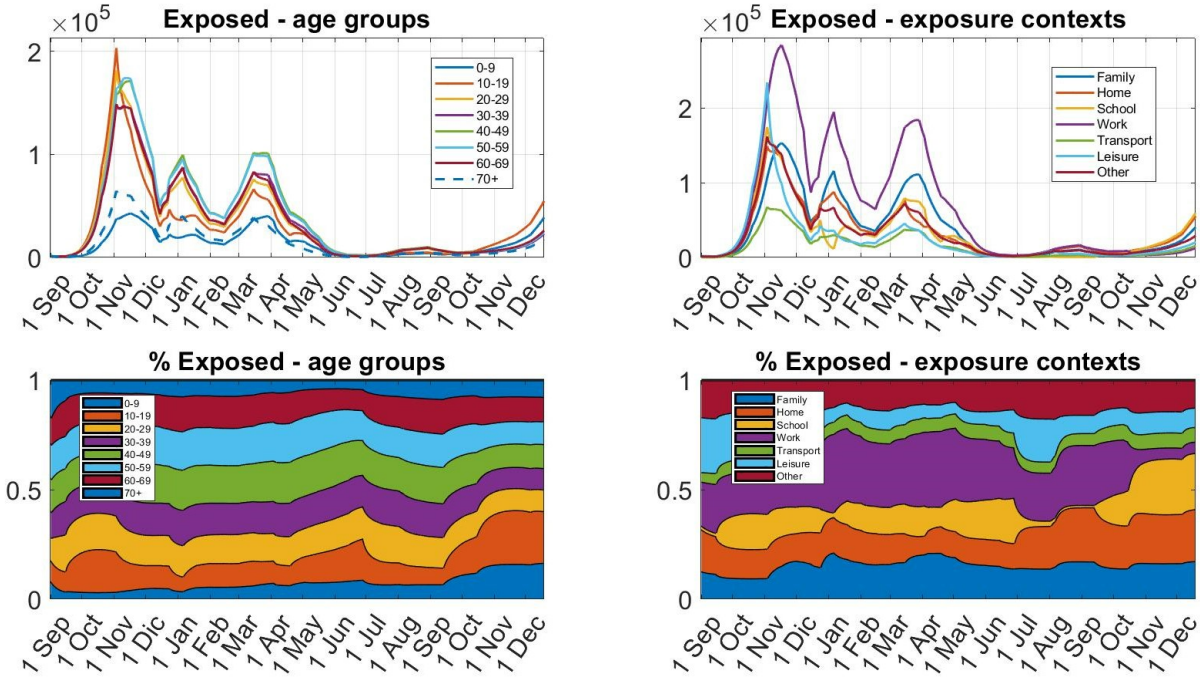

Figure 25: Exposed in Italy with GP containment measures: at the top, evolution of the exposed individuals divided by age group (a) and context of exposition (b); at the bottom, distribution of age groups (c) and contexts of exposition (d) in the exposed compartment.

4 Conclusions and perspectives

We introduced a new mathematical model to describe COVID-19 epidemic in Italy during the years 2020 and 2021. This is a multi-age and multi-context SEIHRDV model, constituted by seven compartments, susceptible individuals S, Exposed individuals E, infectious individuals I, healing individuals H, recovered individuals R, dead individuals D, vaccinated individuals V. This model is able to track the infections patterns among age groups happening in different exposition contexts. In this work, we exploited this model to reconstruct COVID-19 spread in different scenarios between September 2020 and July 2021 in Italy, in Lombardy and in Lazio, and taking into account the vaccination campaign and Green Pass Interventions. This model allows to assess the impact of different NPIs that can be implemented in various contexts heterogeneously. Indeed, we obtained numerical results differentiated for age and context: this was useful to better understand which age groups and contexts of exposition were the most risky.

The model has been validated using data from the Dipartimento di Protezione Civile, Italy, which were also employed to calibrate the model parameters through a standard Least Squares optimization scheme. In this calibration process, we relied on information on deceased individuals, for sure those most reliable and least affected by monitoring uncertainties.

The SEIHRDV multiage and multicontext model provides a valuable framework for analyzing the differing behaviors observed between age groups and understanding how infections spread within various exposure contexts. Nonetheless, further adjustments are needed, such as introducing an additional compartment to account for fully vaccinated individuals or tracking undetected cases, as done in other studies. Despite these limitations, we are confident that this model represents a fundamental tool for policymakers, enabling reliable scenario analyses during epidemic outbreaks.

Acknowledgments

L.D., N.P., and G.Z. acknowledge their membership to INdAM group GNCS – Gruppo Nazionale per il Calcolo Scientifico (National Group for Scientific Computing, Italy). The present reasearch is part of the activities of "Dipartimento di Eccellenza 2023-2027", MUR, Italy, Department of Mathematics, Politecnico di Milano.

References

[1] N. Parolini, G. Ardenghi, L. Dede', and A. Quarteroni. A mathematical dashboard for the analysis of italian COVID-19 epidemic data. *International Journal for Numerical Methods in Biomedical Engineering*, 37(9):e3513, 2021.

[2] W.O. Kermack and A. G. McKendrick. A contribution to the mathematical theory of epidemics. *Proceedings of the royal society of london. Series A, Containing papers of a mathematical and physical character*, 115(772):700–721, 1927.

[3] P. J. Wangersky. Lotka-Volterra population models. *Annual Review of Ecology and Systematics*, 9:189–218, 1978.

[4] N. Parolini, L. Dede', P. Antonietti, G. Ardenghi, A. Manzoni, E. Miglio, A. Pugliese, M. Verani, and A. Quarteroni. SUIHTER: A new mathematical model for COVID-19. Application to the analysis of the second epidemic outbreak in Italy. *Proceedings of the Royal Society A*, 477(2253):20210027, 2021.

[5] G. Dimarco, B. Perthame, G. Toscani, and M. Zanella. Kinetic models for epidemic dynamics with social heterogeneity. *Journal of Mathematical Biology*, 83(1):1–32, 2021.

[6] G. Bertaglia and L. Pareschi. Hyperbolic models for the spread of epidemics on networks: kinetic description and numerical methods. *ESAIM: Mathematical Modelling and Numerical Analysis*, 55(2):381–407, 2021.

[7] E. Bertuzzo, L. Mari, D. Pasetto, S. Miccoli, R. Casagrandi, M. Gatto, and A. Rinaldo. The geography of COVID-19 spread in italy and implications for the relaxation of confinement measures. *Nature Communications*, 11(1):1–11, 2020.

[8] F. Della Rossa, D. Salzano, A. Di Meglio, F. De Lellis, M. Coraggio, C. Calabrese, A. Guarino, R. Cardona-Rivera, P. De Lellis, D. Liuzza, et al. A network model of Italy shows that intermittent regional strategies can alleviate the COVID-19 epidemic. *Nature Communications*, 11(1):1–9, 2020.

[9] M. Gatto, E. Bertuzzo, L. Mari, S. Miccoli, L. Carraro, R. Casagrandi, and A. Rinaldo. Spread and dynamics of the COVID-19 epidemic in Italy: Effects of emergency containment measures. *Proceedings of the National Academy of Sciences*, 117(19):10484–10491, 2020.

[10] E. Loli Piccolomini and F. Zama. Monitoring italian COVID-19 spread by a forced SEIRD model. *PloS one*, 15(8):e0237417, 2020.

[11] V. Ram and L. P. Schaposnik. A modified age-structured SIR model for COVID-19 type viruses. *Scientific Reports*, 11(1):1–15, 2021.

[12] B. Ivorra, M. R. Ferrández, M. Vela-Pérez, and A. M. Ramos. Mathematical modeling of the spread of the coronavirus disease 2019 (COVID-19) taking into account the undetected infections. The case of China. *Communications in Nonlinear Science and Numerical Simulation*, 88:105303, 2020.

[13] A. Comunian, R. Gaburro, and M. Giudici. Inversion of a SIR-based model: A critical analysis about the application to COVID-19 epidemic. *Physica D: Nonlinear Phenomena*, 413:132674, 2020.

[14] G. Bertaglia and L. Pareschi. Hyperbolic compartmental models for epidemic spread on networks with uncertain data: application to the emergence of COVID-19 in italy. *Mathematical Models and Methods in Applied Sciences*, 31(12):2495–2531, 2021.

[15] E. Kuhl. *Computational Epidemiology*. Springer, 2021.

[16] P.E. Lekone and B.F. Finkenstädt. Statistical inference in a stochastic epidemic SEIR model with control intervention: Ebola as a case study. *Biometrics*, 62(4):1170–1177, 2006.

[17] C. Zimmer, R. Yaesoubi, and T. Cohen. A likelihood approach for real-time calibration of stochastic compartmental epidemic models. *PLoS Computational Biology*, 13(1):e1005257, 2017.

[18] N. Hoertel, M. Blachier, C. Blanco, M. Olfson, M. Massetti, M.S. Rico, F. Limosin, and H. Leleu. A stochastic agent-based model of the SARS-CoV-2 epidemic in france. *Nature Medicine*, 26(9):1417–1421, 2020.

[19] C.C. Kerr, R.M. Stuart, D. Mistry, R.G. Abeysuriya, K. Rosenfeld, G.R. Hart, R.C. Núñez, J.A. Cohen, P. Selvaraj, B. Hagedorn, et al. Covasim: an agent-based model of COVID-19 dynamics and interventions. *PLOS Computational Biology*, 17(7):e1009149, 2021.

[20] J. Lasser, J. Sorger, L. Richter, S. Thurner, D. Schmid, and P. Klimek. Assessing the impact of SARS-CoV-2 prevention measures in Austrian schools using agent-based simulations and cluster tracing data. *Nature communications*, 13(1):554, 2022.

[21] K.D. Olumoyin, A.M. Khaliq, and K.M. Furati. Data-driven deep-learning algorithm for asymptomatic COVID-19 model with varying mitigation measures and transmission rate. *Epidemiologia*, 2(4):471–489, 2021.

[22] G. Bertaglia, C. Lu, L. Pareschi, and X. Zhu. Asymptotic-preserving neural networks for multiscale hyperbolic models of epidemic spread. *Mathematical Models and Methods in Applied Sciences*, 32(10):1949–1985, 2022.

[23] S. Shaier, M. Raissi, and P. Seshaiyer. Data-driven approaches for predicting spread of infectious diseases through DINNs: Disease informed neural networks. *Letters in Biomathematics*, 9(1):71–105, 2022.

[24] G. Ziarelli, N. Parolini, and M. Verani. Learning epidemic trajectories through kernel operator learning: from modelling to optimal control. *arXiv preprint arXiv:2404.11130*, 2024.

[25] C. Millevoi, D. Pasetto, and M. Ferronato. A physics-informed neural network approach for compartmental epidemiological models. *PLOS Computational Biology*, 20(9):e1012387, 2024.

[26] G. Ziarelli, S. Pagani, N. Parolini, F. Regazzoni, and M. Verani. A model learning framework for inferring the dynamics of transmission rate depending on exogenous variables for epidemic forecasts. *arXiv preprint arXiv:2410.11545*, 2024.

[27] L. Mari, R. Casagrandi, E. Bertuzzo, D. Pasetto, S. Miccoli, A. Rinaldo, and M. Gatto. The epidemicity index of recurrent SARS-CoV-2 infections. *Nature Communications*, 12(1):1–12, 2021.

[28] V. Marziano, G. Guzzetta, A. Mammone, F. Riccardo, P. Poletti, F. Trentini, M. Manica, A. Siddu, A. Bella, P. Stefanelli, et al. The effect of COVID-19 vaccination in Italy and perspectives for living with the virus. *Nature Communications*, 12(1):1–8, 2021.

[29] G. Giordano, M. Colaneri, A. Di Filippo, F. Blanchini, P. Bolzern, G. De Nicolao, P. Sacchi, P. Colaneri, and R. Bruno. Modeling vaccination rollouts, SARS-CoV-2 variants and the requirement for non-pharmaceutical interventions in Italy. *Nature Medicine*, 27(6):993–998, 2021.

[30] J. Mossong, N. Hens, M. Jit, P. Beutels, K. Auranen, R. Mikolajczyk, M. Massari, S. Salmaso, G. S. Tomba, J. Wallinga, et al. Social contacts and mixing patterns relevant to the spread of infectious diseases. *PLoS Medicine*, 5(3):e74, 2008.

[31] G. Giordano, F. Blanchini, R. Bruno, P. Colaneri, A. Di Filippo, A. Di Matteo, and M. Colaneri. Modelling the COVID-19 epidemic and implementation of population-wide interventions in Italy. *Nature medicine*, 26(6):855–860, 2020.

[32] M. Chinazzi, J. T. Davis, M. Ajelli, C. Gioannini, M. Litvinova, S. Merler, A. Pastore y Piontti, K. Mu, L. Rossi, K. Sun, et al. The effect of travel restrictions on the spread of the 2019 novel coronavirus (COVID-19) outbreak. *Science*, 368(6489):395–400, 2020.

[33] F. Brauer, P. Van den Driessche, J. Wu, and L. Allen. *Mathematical Epidemiology*, volume 1945. Springer, 2008.

[34] G. Ziarelli, L. Dede', N. Parolini, M. Verani, and A. Quarteroni. Optimized numerical solutions of SIRDVW multiage model controlling SARS-CoV-2 vaccine roll out: An application to the italian scenario. *Infectious Disease Modelling*, 8(3):672–703, 2023.

[35] J. Shapiro, N.E. Dean, Z.J. Madewell, Y. Yang, M.E. Halloran, and I. Longini. Efficacy estimates for various COVID-19 vaccines: what we know from the literature and reports. *MedRxiv*, 2021.

[36] P. Poletti, M. Tirani, D. Cereda, F. Trentini, G. Guzzetta, V. Marziano, S. Buoro, S. Riboli, L. Crottogini, R. Piccarreta, et al. Age-specific SARS-CoV-2 infection fatality ratio and associated risk factors, Italy, February to April 2020. *Eurosurveillance*, 25(31):2001383, 2020.

[37] N. Brazeau, R. Verity, S. Jenks, H. Fu, C. Whittaker, P. Winskill, I. Dorigatti, P. Walker, S. Riley, R. P. Schnekenberg, et al. COVID-19 infection fatality ratio: estimates from seroprevalence. *Supplementary data–report 34, London: Imperial College*, 2020.

[38] F. Zhou, T. Yu, R. Du, G. Fan, Y. Liu, Z. Liu, J. Xiang, Y. Wang, B. Song, X. Gu, et al. Clinical course and risk factors for mortality of adult inpatients with COVID-19 in Wuhan, China: a retrospective cohort study. *The Lancet*, 395(10229):1054–1062, 2020.

[39] N. Parolini, L. Dede', G. Ardenghi, and A. Quarteroni. Modelling the COVID-19 epidemic and the vaccination campaign in italy by the suihter model. *Infectious Disease Modelling*, 7(2):45–63, 2022.

[40] S. Y. Del Valle, J. M. Hyman, and N. Chitnis. Mathematical models of contact patterns between age groups for predicting the spread of infectious diseases. *Mathematical Biosciences and Engineering: MBE*, 10:1475, 2013.

[41] Presidenza del Consiglio dei Ministri, Comitato Tecnico Scientifico. Report n°57. 28 April 2020.

[42] J. Zhang, M. Litvinova, Y. Liang, Y. Wang, W. Wang, S. Zhao, Q. Wu, S. Merler, C Viboud, A. Vespignani, et al. Changes in contact patterns shape the dynamics of the COVID-19 outbreak in China. *Science*, 368(6498):1481–1486, 2020.

[43] E.J. Emanuel, J.P. Philips, and S. Popescu. Covid-19 Activity Risk Levels. July 2020.

[44] A. Summan and A. Nandi. Timing of non-pharmaceutical interventions to mitigate COVID-19 transmission and their effects on mobility: a cross-country analysis. *The European Journal of Health Economics*, 23(1):105–117, 2022.

[45] Istituto Superiore di Sanità. Epidemia COVID-19. aggiornamento nazionale 10 novembre 2021. November 2021.

MOX Technical Reports, last issues

Dipartimento di Matematica
Politecnico di Milano, Via Bonardi 9 - 20133 Milano (Italy)

108/2024 Arostica, R.; Nolte, D.; Brown, A.; Gebauer, A.; Karabelas, E.; Jilberto, J.; Salvador, M.; Bucelli, M.; Piersanti, R.; Osouli, K.; Augustin, C.; Finsberg, H.; Shi, L.; Hirschvogel, M.; Pfaller, M.; Africa, P.C.; Gsell, M.; Marsden, A.; Nordsletten, D.; Regazzoni, F.; Plank, G.; Sundnes, J.; Dede', L.; Peirlinck, M.; Vedula, V.; Wall, W.; Bertoglio, C.
A software benchmark for cardiac elastodynamics

109/2024 Liverotti, L.; Ferro, N.; Matteucci, M.; Perotto, S.
A PCA and mesh adaptation-based format for high compression of Earth Observation optical data with applications in agriculture

110/2024 Pederzoli, V.; Corti, M.; Riccobelli, D.; Antonietti, P.F.
A coupled mathematical and numerical model for protein spreading and tissue atrophy, applied to Alzheimer's disease

107/2024 Chen, J.; Ballini, E.; Micheletti, S.
Active Flow Control for Bluff Body under High Reynolds Number Turbulent Flow Conditions Using Deep Reinforcement Learning

106/2024 Brunati, S.; Bucelli, M.; Piersanti, R.; Dede', L.; Vergara, C.
Coupled Eikonal problems to model cardiac reentries in Purkinje network and myocardium

105/2024 Bartsch, J.; Barakat, A.A.; Buchwald, S.; Ciaramella, G.; Volkwein, S.; Weig, E.M.
Reconstructing the system coefficients for coupled harmonic oscillators

104/2024 Cerrone, D.; Riccobelli, D.; Vitullo, P.; Ballarin, F.; Falco, J.; Acerbi, F.; Manzoni, A.; Zunino, P.; Ciarletta, P.
Patient-specific prediction of glioblastoma growth via reduced order modeling and neural networks

103/2024 Fois, M.; Gatti, F.; de Falco, C.; Formaggia, L.
A comparative analysis of mesh-based and particle-based numerical methods for landslide run-out simulations

101/2024 Bonetti, S.; Corti, M.
Unified discontinuous Galerkin analysis of a thermo/poro-viscoelasticity model

102/2024 Bucelli, M.
The lifex library version 2.0